A novel approach for mitigating power quality issues in a PV integrated microgrid system using an improved jelly fish algorithm

Swati Suman[1*], Debashis Chatterjee[2], Rupali Mohanty[3]

[1,2,3] Department of Electrical Engineering, Jadavpur University, Kolkata-700032, West Bengal, India

A B S T R A C T

A two-step methodology was used to address the power quality concerns for the PV integrated microgrid system. In the first step, partial shading was included to deal with the real-time issues. The Improved Jelly Fish Algorithm integrated Perturb and Observb (IJFA-PO) has been proposed to track the Global Maximum Power Point (GMPP). In the second step, the main unit powered by a DC-AC converter is synchronised with the grid. To cope with the wide voltage variation, an auxiliary unit is connected to the main unit in the opposite phase. This study evaluates various switching approaches to determine the optimal solution for achieving the stated goals. It was found that the IJFA-based SHE in 120^o conduction gives improved results. A novel series compensation technique has been employed to further eliminate harmonics before grid integration. The proposed IJFA has been used to determine the switching angles for the SHEPWM converter. The objective function and novel series compensation work together to determine the harmonics that should be decreased and kept to a minimum. Three switching angles' performance was equivalent to that of nine switching angles. As a result, higher-order harmonics can be minimised with fewer switches, and switching losses can be lowered without compromising efficiency. The THD of the proposed system was 1.32 percent, which is very much within the tolerable limit of IEEE 1547, IEC, and CIGRE WG 36-05 standards. In terms of efficiency, metaheuristics, and convergence, the proposed system outperformed the existing ones. The model was developed in MATLAB/Simulink 2016b. To verify the simulation results, an experimental prototype of grid synchronised PV capacity of 260W was tested under various loading conditions. The present model is reliable and features a simple controller that provides more convenient and adequate performance for practical reasons.

Keywords: Harmonic mitigation, Selective Harmonic Elimination Pulse Width Modulation (SHEPWM) inverters, Search-based optimization techniques, Total Harmonic Distortion (THD), Modulation Indices (MI)

1. Introduction

Solar energy is always a viable option for meeting power demands. Its clean and green features, easy accessibility, and cost-free nature have made it extremely popular [1].

There are numerous challenges, such as properly tracking MPP in non-uniform conditions and injecting harmonics-free voltage into the grid. Traditional approaches such as Incremental Conductance (IC) [2], Hill Climbing (HC), Perturb and Observb (P&O) [3], etc., is incapable of tracking MPP under Partial Shading Conditions (PSC). Many metaheuristic strategies, including Particle Swarm Optimization (PSO) [4], Jaya algorithm [5], Whale Optimization Algorithm (WOA) [6], Grey Wolf Optimization (GWO) [7], and Jelly Search Algorithm (JSA) [8-11], have been utilised to overcome the challenges produced by PSC. To address this problem, a hybrid Improved Jelly Fish Algorithm integrated Perturb and Observb (IJFA-PO) method was proposed, which combines the benefits of both traditional and innovative methods.

The choice of a proper converter is mandatory because it can reduce undesirable harmonics in order to deliver power efficiently to the grid. This paper undergoes comparative analysis of several switching techniques to get a better picture. Voltage source inverters are commonly used with renewable energy sources. The SPWM [12], conventional 180^o and 120^o, was used in a hybrid system with the Biogeography-Based Algorithm (BBO) and the Unified Power Quality Conditioner (UPQC) [13]. To validate effective harmonic mitigation for the present model, the proposed IJFA was used to produce firing angles for SHE based 180^o and 120^o switching approaches.

Power quality was improved using a Radial Basis Function Neural Network (RBFNN) integrated with a Proportional Integral (PI) controller [14]. A Field Programmable Gate Array (FPGA) approach was employed to minimise low order harmonics in fundamental switching frequency modulation for PV application [15]. For harmonic removal in multilevel inverters, a modified Newton Raphson (MNR)

and pattern recognition were utilised [16]. The SHEPWM and Selective Harmonic Mitigation PWM (SHMPWM) based three-level NPC converters were employed, applying the harmonic suppression algorithm [17]. In [18], an Artificial Bee Colony (ABC) and filter compensation modules were used to minimise harmonics in microgrids [19].

The typical SHE-PWM approach was found incapable of regulating the non-eliminated harmonics, resulting in higher values [20-21]. As per the literature, direct solutions suffer from computational complexity and weaker convergence. Furthermore, a higher number of harmonics to be removed necessitates a large number of switching angles, which adds computational complexity and losses unnecessarily. The proposed search-based SHEPWM technique has addressed this problem by providing optimum angles for a main and auxiliary inverter. Three switching per quarter cycle was employed to minimise harmonics using the proposed IJFA metaheuristic-based SHEPWM approach. The optimised three switching angles per quarter cycle have the same performance as that of nine firing angles but with reduced losses as found in the latter case. As a result of this novel concept, switching losses are reduced, and the converter's life is extended.

To eliminate undesired harmonics, a series compensation network was used on the grid side in this paper. It would also meet grid demand and maintain voltage supply in the event of a wider voltage variation, dip or unbalance. On applying the proposed model, the harmonics were minimised drastically and the THD was determined to be just 1.32 percent, which is within the IEEE 1547, IEC, CIGRE WG 36-05 standards [22-25]. A piecewise mixed model technique was adopted to store the set of switching angles offline and use them for practical applications [26].

This paper has been divided into various sections. The suggested strategy is described in Section 2. The third section delves into the various switching techniques in depth. In section 4, the proposed compensation mechanism based on IJFA was detailed. The PSC is further discussed in Section 5. The control scheme is developed in Section 6. The results and comments are presented in Section 7. Last but not least, section 8 depicts the conclusion.

2. Proposed Scheme

Due to PSC and variation in isolation, it is difficult to maintain the DC bus and output voltage using a single DC-DC boost converter. Various literature is cited which implies difficult control methods, slower MPP tracking, and expensive implementation costs. Furthermore, if the input voltage is low, an additional Boost converter will be required to manage the entire power, increasing the overall cost and decreasing reliability. The prototype shown in this work is robust, non-bulky, low-cost, and simple to deploy.

The aforementioned concerns are addressed by a novel low-rated auxiliary unit integrated series compensation network on the ac side, which mitigates voltage demands and stabilizes the output ac voltage of the inverter. It also effectively eliminates harmonics with fewer switching angles and a single boost converter, addressing all of the aforementioned issues. The proposed prototype's layout is shown in Figure 1. The primary PV panel is the supply panel, whereas the auxiliary panel is the compensatory panel. The primary PV panel is under partially shaded conditions. The auxiliary unit's ratings are 20 percent of the main unit's. The main PV panel is coupled to the DC-DC boost converter, which supplies the grid-synchronized inverter. The proposed IJFA-PO technique computes the duty cycle for boost converter operation, which monitors the GMPP smoothly among all the local peaks at a quicker rate. The voltage is three times that of the PV voltage, making it ideal for grid synchronization but it has some limits. The greater ratio is attainable at the expense of decreased power output, which compromises the system's reliability.

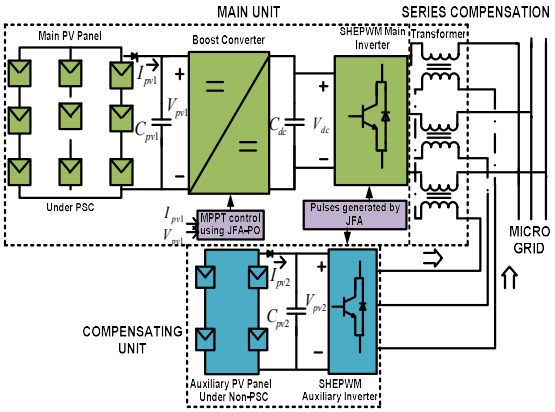

Figure 1 Proposed prototype

As shown in Figure 1, the auxiliary panel can directly feed the compensating inverter connected to the main inverter through a series compensating transformer. To identify the optimal performance for the proposed system, different switching strategies (180º conventional, IJFA implemented in 180º, 120º conventional, IJFA implemented in 120º, SPWM) were compared. It was found that IJFA based 120º produced improved results. These inverters were switched at a low frequency. The proposed IJFA uses three switching angles for each inverter to drive them in the 120º SHE implemented mode. The performance of the optimised three switches per quarter cycle was better than the nine switching angles. As a result, switching losses are reduced, and the converter's life and efficiency are increased. The main inverter has three switching angles that minimise harmonics (5th, 7th, 11th, 23rd), but other higher-order harmonics up to 29th will remain. In this paper, harmonics up to the 29th order are considered. The auxiliary inverter deals with these harmonics in 180° phase opposition, and the output voltage THD would be decreased greatly as a result. A piecewise mixed model was used in which the switching angles were stored offline for online implementation.

3. Different switching techniques for harmonic elimination

3.1 Sinusoidal Pulse Width Modulation Inverter

The two types of multilevel modulation methods are high switching frequency and fundamental switching control, in which SPWM and Space Vector PWM fall within the former. One of the primary challenges with high-power applications such as SPWM inverters is power dissipation. If the output voltage levels are considered to be "n," then "n-1" can be used to find the carrier waves. The output SPWM inverter in this paper is developed for two levels, as illustrated in Figure 2. A Phase Lock Loop (PLL) was used for controlling purposes. The modulation index can be adjusted to modify the RMS value of the output voltage. If the value of M is chosen carefully, it can reduce or eliminate harmonics to a great extent, which reduces the THD.

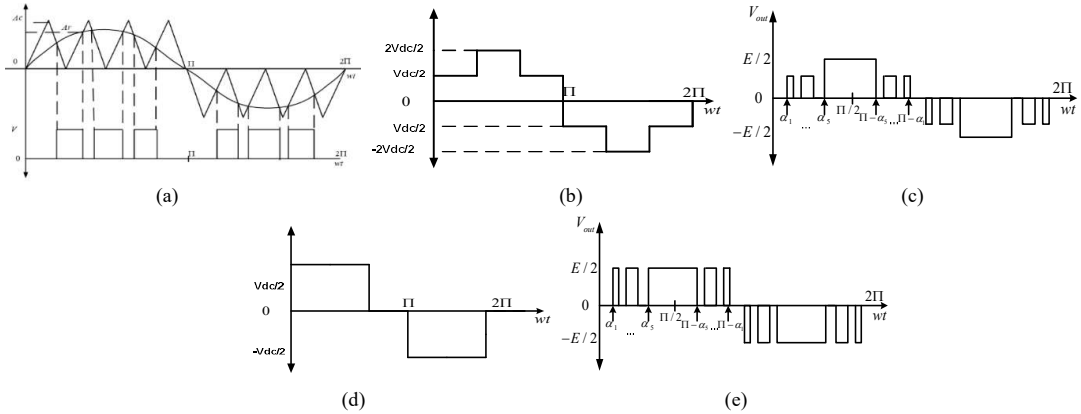

Figure 2. Pulse generation for a) SPWM b) 180º conventional c) IJFA implemented in 180º d) 120º conventional e) IJFA implemented in 120º

The output voltage in quasi sine wave form can be written in terms of Fourier series.

$$V_{an} = a_0/2 + \sum_{n=1}^{\infty}(a_n \cos(nwt) + b_n \sin(nwt)) \quad (1)$$

As the waveform has symmetry of quarter-wave therefore, a_0 and a_n =0 for all values of n, b_n=0 for all even values of n; n is the harmonic order, $\alpha_1 ... \alpha_n$ are the switching angles. $f(wt)$ was taken from the waveform shown in Fig 2a.

3.2 Using the direct solution method for the conventional 180° switching strategy

$$b_n = 4/\Pi\left[\int_0^{\Pi/2} f(wt)\sin(nwt)d(wt)\right] \quad (2)$$

$$b_n = \left(4/\Pi\right)\left[\int_0^{\Pi/3}\frac{V_{dc}}{3}\sin(nwt)d(wt) + \int_{\Pi/3}^{\Pi/2}\frac{2V_{dc}}{3}\sin(nwt)d(wt)\right] \quad \text{(delay of 0°)} \quad (3)$$

$$b_n = \left(4V_{dc}/3n\Pi\right)\left[\left[-\cos(nwt)\right]_0^{\Pi/3} + 2\left[-\cos(nwt)\right]_{\Pi/3}^{\Pi/2}\right]$$

$$\text{Onsolving, } b_n = \left(4V_{dc}/3n\Pi\right)\left[1 + \cos\left(\frac{n\Pi}{3}\right)\right] \quad (4)$$

$$V_{an} = \left(4V_{dc}/3n\Pi\right)\left[1 + \cos\left(\frac{n\Pi}{3}\right)\right]\sin(nwt) \text{ with a phase of } \Phi_n = \tan^{-1}(a_n/b_n) = 0 \quad (5)$$

3.2.1 SHE implemented using the proposed IJFA in a conventional 180° switching strategy

With a proper selection of three switching's per quarter cycle from the optimization technique, the harmonics up to 29th order were mitigated. $f(\alpha)$ was analysed from the unipolar waveform shown in Fig 2b.

$$b_n = \left(4/\Pi\right)\int_0^{\Pi/2} f(\alpha)\sin(n\alpha)(d\alpha) \quad \text{(by using (1))} \quad (6)$$

$$b_n = \left(4/n\Pi\right)\left[\int_{\alpha_1}^{\alpha_2}\frac{V_{dc}}{3}\sin(n\alpha)(d\alpha) + \int_{\alpha_3}^{\alpha_4}\frac{V_{dc}}{3}\sin(n\alpha)(d\alpha) + \int_{\alpha_5}^{\Pi/2}\frac{2V_{dc}}{3}\sin(n\alpha)(d\alpha)\right] \quad (7)$$

$$\text{On solving, } b_n = \left(4V_{dc}/3n\Pi\right)\left[\cos(n\alpha_1) - \cos(n\alpha_2) + \cos(n\alpha_3) - \cos(n\alpha_4) + 2\cos(n\alpha_5)\right]$$

$$b_n = \left(4V_{dc}/3n\Pi\right)\left[-\sum_{k=1}^{m}(-1)^k\cos(n\alpha_k) - 2\sum_{k=m+1}^{m}(-1)^k\cos(n\alpha_k)\right] \text{where } 0 < \alpha_1 < \alpha_2 ... < \alpha_5 < \Pi/2$$

(8)

3.3 Using the direct solution method for the conventional 120° switching strategy

$$b_n = 4/\Pi\left[\int_{\Pi/6}^{\Pi/2}\frac{V_{dc}}{2}\sin(nwt)d(wt)\right] \quad \text{(by using (1) and considering a delay of 30° in the limits)}$$

(9)

$$\text{On solving, } b_n = 2V_{dc}/n\Pi\left[\cos(nwt)\right]_{\Pi/2}^{\Pi/6} \quad (10)$$

$$V_{an} = {}^{2V_{dc}}\!/_{n\Pi} \sin\left(\frac{n\Pi}{2}\right)\sin\left(\frac{n\Pi}{3}\right)\sin(nwt) \text{ at a phase angle of } \phi_n = \tan^{-1}\left({}^{a_n}\!/_{b_n}\right) \quad (11)$$

3.3.1 SHE implemented using the proposed IJFA in a conventional 120° switching strategy

$$b_n = \left({}^{4}\!/_{\Pi}\right)\int_{x}^{{}^{\Pi}\!/_{2}} f(\alpha)\sin(n\alpha)(d\alpha), \text{ (x>0 is the delay according to the search-based SHE)} \quad (12)$$

$$b_n = \left({}^{4}\!/_{\Pi}\right)\left[\int_{\alpha_1}^{\alpha_2}\frac{V_{dc}}{2}\sin(n\alpha)(d\alpha) + \int_{\alpha_3}^{\alpha_4}\frac{V_{dc}}{2}\sin(n\alpha)(d\alpha) + \int_{\alpha_5}^{{}^{\Pi}\!/_{2}}\frac{V_{dc}}{2}\sin(n\alpha)(d\alpha)\right] \quad (13)$$

on solving, it can be written as

$$b_n = -\frac{4}{n\pi}\sum_{k=1}^{m}(-1)^k \cos n\alpha_k \text{ where } 0 < \alpha_1 < \alpha_2 ... < \alpha_5 < {}^{\Pi}\!/_{2} \quad (14)$$

Due to the symmetrical nature of unipolar line to line voltage, triplen harmonics are absent in a three-phase balanced system. The + and – signs of cos denote the rising and falling edges in the transition phases. The switching angles can be determined by expanding and equating voltage harmonics (10) and (14) to zero and setting the fundamental component to MI, where (MI<1). The optimised angles with the lowest THD were chosen as they reduce harmonics introduced to the grid. The presence of trigonometric terms increases the complexity as it produces multiple or no solutions at all. To solve the non-linear equations acquired through direct solution or conventional technique, IJFA-based SHE comes into the picture. The existing solutions are discontinuous at some points, which requires an increased number of switching angles to reduce harmonics. Lower switching rates are preferred since they result in fewer switching losses and higher efficiency. IJFA reduces overall THD by mitigating a wider spectrum of harmonics with only three optimum angles. These angles are calculated offline and stored in the lookup table memory of the Digital Signal Processor (DSP) for online use. The angles obtained for the lowest voltage THD to the closed point of MI are used to determine linearity. As a result, the SHE technique was used to overcome the problem of discontinuity.

4. A Proposed compensation technique using the Improved Jelly Fish Algorithm (IJFA)

Jui-Sheng Chou and Dinh-Nhat Truong developed JFA in 2021 which is inspired by jellyfish searching for food in the ocean. Three strategies are used by the jellyfish search optimizer. (i) Jellyfish move with the ocean current or within the group; (ii) Jellyfish are drawn to areas with more food; and (iii) the amount of food is assigned and the appropriate fitness function (FF) is computed. The heavy active and passive movements of the jellyfishes within the swarm cause a jellyfish bloom. When food sizes are compared, the optimum placements can be determined and the FF's best value may be evaluated. As a result, JFA can be modelled as

$$\overrightarrow{X_{i+1}} = \eta\vec{X}_i(1-\vec{X}_i), 0 \le \vec{X}_0 \le 1 \quad (15)$$

$$\vec{X}_i(t+1) = \vec{X}_i(t) + \vec{r}.*(\vec{X}^* - \beta * r_1 * \mu) \quad (16)$$

Where the value for η is taken as 4; $\vec{X}_i$ is a vector that contains the logistic chaotic values of the ith jellyfish; $\vec{X}_0$ is an initial vector of jellyfish 0, generated randomly between [0, 1]; $\vec{X}^*$ is the location with the most food;.∗ is the element-by-element vector multiplication; β > 0 is the distribution coefficient taken as β = 3; μ is the mean of the population and r ,r_1, r_2, r_3 is a random number between [0, 1]; $\vec{X}_i(t+1)$ is the ocean current in (16). The movements of jellyfish inside the swarm are controlled by passive and active motions. Jellyfish move about their positions in passive motion, and the fresh update of their positions is described by using (17). The active motion, on the other hand, is determined according to the formula shown in (18).

$$\overrightarrow{X}_i(t+1) = \overrightarrow{X}_i(t) + r_3 * \gamma * (U_b - L_b) \tag{17}$$

$$\overrightarrow{X}_i(t+1) = \overrightarrow{X}_i(t) + \vec{r} * \overrightarrow{D} \tag{18}$$

where γ > 0 indicates the length of the motion around the current location. U_b and L_b are the upper and the lower bound of the search space of the problem, respectively. $\vec{D}$ is used to determine the direction of the motion of the current jellyfish within the next generation. This motion corresponds to the tracking of the best food position and is expressed in (19). Where j is the index of a jellyfish selected randomly, and FF indicates the fitness function.

$$\begin{aligned} &\overrightarrow{D} = \overrightarrow{X}_i(t) - \overrightarrow{X}_j(t); if, FF(\overrightarrow{X}_i(t)) < FF(\overrightarrow{X}_j(t)) \\ &\overrightarrow{D} = \overrightarrow{X}_j(t) - \overrightarrow{X}_i(t); otherwise \end{aligned} \tag{19}$$

The $c(t)$ is used to switch between ocean currents, passive and active motions, all of which may be described mathematically in (20).

$$c(t) = \left(1 - {}^{t}\!\!\diagup\!\!{}_{t_{\max}}\right) * (2 * r - 1) \tag{20}$$

where t is the current evaluation; $t_{\max}$ is the maximum evaluation A jellyfish swarm is formed over time, and each jellyfish continues to migrate within the swarm to obtain a better position, using both active and passive motions, resulting in exploitation at this stage. Meanwhile, $c(t)$ switches between these motions. The user should choose between two control options i.e., pop and $t_{\max}$. As per the latter, fewer settings are required, resulting in less labour and haphazard trials to fine-tune the JFA's performance.

4.1 The proposed IJFA

The JFA algorithm's exploitation capability was found to be low due to the current jellyfish movement within the population. This slowed the convergence toward the best solution so far, resulting in a long time to find a better solution. Furthermore, local exploration capability searches multiple rounds within the regions where the swarm's presence is limited. As a result, looking for areas inside the swarm that haven't been investigated by any of the other jellyfish helped to fetch better results. When the control variable r is small, the Improved Jelly Fish Algorithm (IJFA) explores around the best-so-far solution, but when r is large, it improves exploration around the swarm for reaching other regions. As a result, the proposed IJFA equation is as follows:

$$\overrightarrow{X_i}(t+1) = \overrightarrow{X}_i(t) + r * (\overrightarrow{X}_{r1}(t) - \overrightarrow{X}_{r2}(t)) + (1-r)(X * - \overrightarrow{X}_{r3}(t)) \tag{21}$$

where r_1, r_2, and r_3 are the indices of three solutions picked arbitrarily from the population ranging between [0,1]; r is the control parameter which is used to control in moving of the current solution. If r is small, the current solution will be moved to a location located between the best-so-far and $\overrightarrow{X}_{r3}(t)$ to accelerate convergence, if r is high, the current one is updated using two randomly chosen solutions from the population to improve the algorithm's ability to reach new regions. This method is then combined with the JS to modify its performance to reach better solutions in fewer iterations. The proposed IJFA approach for the current scheme is given in the flowchart in Figure 3.

4.1.1 Angle obtained in detail for the main SHEPWM inverter

The proposed IJFA-based SHEPWM technique was used to determine the angle generation for the primary inverter. Three switching angles were found by equating the fundamental component to MI and the rest voltage harmonics to zero, as indicated earlier in (3). A search-based technique has been used to obtain angles and store them offline in the microcontroller memory (25). The three angles can attenuate harmonics up to the 5^{th}, 7^{th}, 11^{th},... 23^{rd} order, but higher-order harmonics such as the 25^{th},...

29th, and so on will still exist. As a result, an auxiliary inverter was used to implement novel series compensation to attenuate existing higher-order harmonics.

4..1.2 Angle calculation for auxiliary SHEPWM inverter to suppress higher orders in detail

As SHEPWM involves trigonometric concepts, it has limits in terms of displaying many solutions. Therefore, to achieve convergence variables must be chosen at the exact point. To avoid the difficulty of finding a solution to a non-linear equation, the problem was changed to an optimization function $t_1(\alpha)$ .The THD obtained should be a minimum (24) and the corresponding angles are to be considered further. The objective function used to produce the angles for the auxiliary inverter for decreasing the existing dominating harmonics

$$t(\alpha) = K_1 * (b_1 - M)^2 + K_5 * \varepsilon_2^2 + ... + K_n * \varepsilon_n^2 \quad (22)$$

Subjected to $0 < \alpha_1 < \alpha_2 .... < \alpha_m < \Pi/2$ (23)

where, $K_1 ... K_n$ are the weights that are applied to the harmonics to be minimized priority-wise, $\varepsilon_1 ... \varepsilon_n$ are the values that are set according to the magnitude of the respective harmonic that is to be reduced. Normally, it is set to zero but here it is taken according to the amount in which the higher-order harmonics are to be reduced. The values of $K_1 ... K_n$ in (22) have to be selected wisely to reduce the magnitude of the harmonics with $\varepsilon_1 ... \varepsilon_n$ amount respectively. As an example, suppose the harmonic amplitudes of the 25th and 29th harmonics are 23 percent and 14 percent, respectively. For reducing the amplitude of the harmonics, the weights must be used in order of priority, with the 25th priority being given first, followed by the 29th. To cancel out the 25th harmonic, it must be set to a value of 23 percent but in the opposite phase. This also applies to any harmonic order of any amplitude. The proposed IJFA algorithm includes the objective function (22) for reducing existing dominating harmonics in particular. The technique was repeated until the desired outcome and convergence were achieved. The angles obtained in the proposed IJFA-based SHEPWM approach (22) should strictly follow the criteria illustrated in (23). As indicated in Figure 1, the three angles achieved are sent to the auxiliary inverter, which undergoes series compensation with the main unit. For a three-phase system, IJFA mitigates a wider range of harmonics (5th ..., 23rd) with only three optimum angles, while others up to 29th are minimised by employing (22) and (23) in IJFA and series compensation technique, thus lowering overall THD. These angles are calculated offline and stored in the lookup table memory of the Digital Signal Processor (DSP) for online use. The objective function (22) was used to minimise the three-phase output voltage THD (24).

$$\%THD = \sqrt{\frac{b_5^2 + b_7^2 + ... + b_{29}^2}{b_1^2}} \quad (24)$$

5. Partial Shading Condition (PSC) tackled through proposed IJFPO-PO

PSC is caused by passing clouds, building shadows, neighbouring trees, bird excreta, and other factors. The efficiency of PV is affected by many peaks and non-convex features. The array consists of modules with solar irradiation of 250 (shaded), 1000 (non-shaded), 800, 1000 W/m2 at a module temperature of 25°C. Under uniform irradiation, simple P&O is effective. However, under non-uniform irradiance, it is unable to track the GMPP among the numerous LMPPs, and the speed drops. As a result, integration of IJFA and PO is carried out to address these scenarios, as shown in Figure 4.

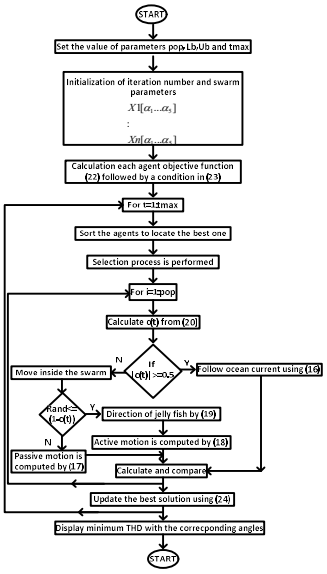

Figure 3. Flowchart for the IJFA

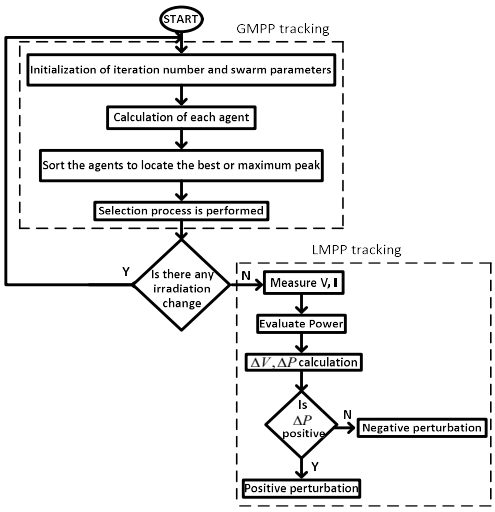

Figure 4. Flowchart of the IJFA-PO

6. Implementation of the control technique

Piecewise mix model equations have been used to store the set of switching angles produced by IJFA. This control method makes use of a set of linear and nonlinear equations that were computed offline using the proposed IJFA and then stored in the processor memory for online usage (25). When compared to other existing strategies, this processor takes little memory space and has a lower computational complexity. Figure 5 depicts the fluctuation of triggering angles with various modulation indices in this method.

For, $0.5 \le \mathrm{MI} \le 0.7$

$$\alpha_1 = -110MI + 95.33,$$
$$\alpha_2 = -140MI + 117.33,$$
$$\alpha_3 = -160MI + 136,$$
$$\alpha_4 = -150MI + 133.67,$$
$$\alpha_5 = -190MI + 162.67$$

For, $0.71 \le \mathrm{MI} \le 0.9$

$$\alpha_1 = 500MI^2 - 880MI + 389,$$
$$\alpha_2 = 450MI^2 - 815MI + 370,$$
$$\alpha_3 = -100MI^2 - 50MI + 38, \quad (25)$$
$$\alpha_4 = 150MI^2 - 350MI + 201.5$$
$$\alpha_5 = 438MI^2 - 784.3MI + 362.39$$

Figure 5 depicts the control system in which the SHEPWM main inverter's three-phase voltage is compared to an appropriate reference output voltage. The error is processed by the PI controller that has been set up to generate MI. The set of triggering angles in the form of equations is stored for different values of MI, and the SHEPWM inverters are triggered by the pulses generated by the driver circuit using that set of equations.

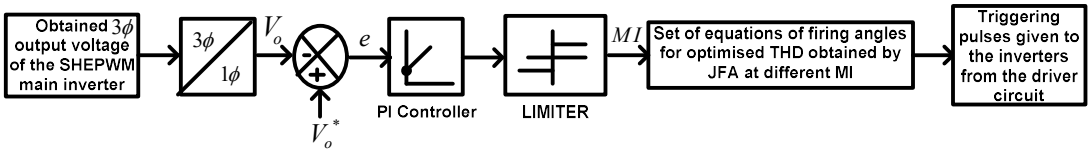

Figure 5. Control unit

7. Result analysis

The model was developed in the MATLAB/Simulink 2016b environment. Figure 6(a) depicts MPP tracking under partially shaded conditions. The grid voltage is depicted in Figure 6(b). It was found that the corresponding algorithm has fewer tuning variables and is easier to implement with a tracking time of 0.01sec. Table 1 shows the results of a comparative analysis of various MPPT approaches.

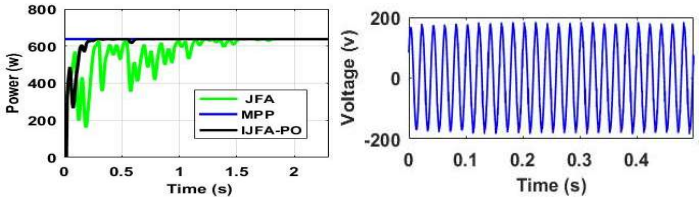

(a) (b)

Figure 6. (a) PSC power curve versus time; (b) System voltage at the grid side

Table 1 A comparison of the proposed MPPT techniques with the existing MPPT techniques

MPPT	Complexity	Tracking under PSC	Dynamic performance	Tracking Speed	Accuracy	Efficiency (%)
P&O	Easy	No	Poor	Low	Less	95.7%
JFA	Easy	Yes	Moderate	Moderate	Moderate	97%
IJFA-PO	Moderate	Yes	Excellent	High	High	99.9%

Figure 7 shows the output waveform of voltage at the main inverter side using the SPWM, conventional 180°, IJFA implemented in 180°, conventional 120°, IJFA implemented in 120°. Figure 8(a) shows the FFT analysis for each output voltage before and after compensation. Figure 8(b) shows the FFT analysis after compensation. It was found that the IJFA, implemented in 120° conduction, has given superior results. The values are obtained by using (22) in opposition to cancelling out the existing dominant harmonics. Three switching angles were generated by the IJFA based SHEPWM technique, used for the main and compensating SHEPWM inverters at a modulation index of 0.85, as indicated in Table 2. The comparison of various bio-inspired algorithms has been done in Figure 8 (c), in which IJFA has given better results for the given plot. The behaviour of triggering pulses over MI has been given in Figure 8 (d). The optimised pulses give better results than the conventional ones.

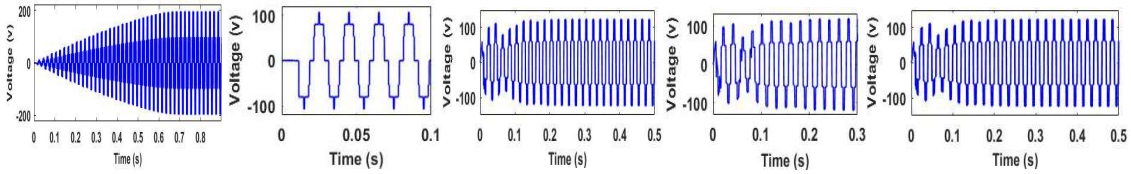

(a) (b) (c) (d) (e)

Figure7. Voltage waveform for unipolar switching at the main inverter side a) SPWM b) 180° conventional c) IJFA implemented in 180° d) 120° conventional e) IJFA implemented in 120°

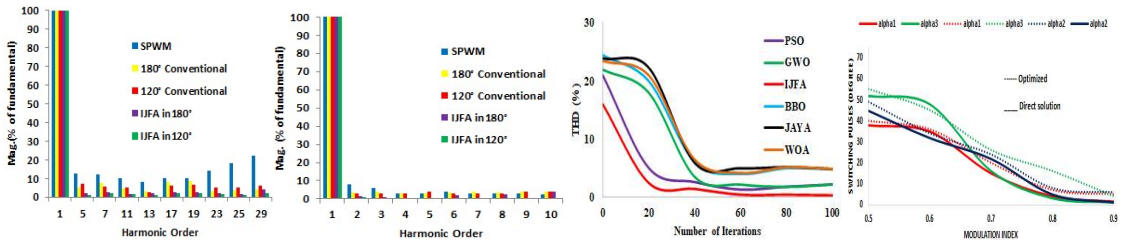

(a) (b) (c) (d)

Figure 8. Analysis of system output a) FFT analysis of the main SHEPWM inverter b) FFT analysis at the grid side c) voltage THD variation over iterations for various metaheuristic techniques d) Switching angle behaviour vs. MI for conventional and optimised pulses

Table 2 Switching angles obtained for different values of firing angles

N	α_1	α_2	α_3	α_4	α_5	α_6	α_7	α_8
3	18.67	23.98						
5	10.45	16.32	22.3	26.56				
7	4.32	8.12	19.67	26.54	30.43	32.85		
9	17.89	25.7	33.62	35.47	39.9	42.2	48.39	52.52

The behaviour of three switching angles per quarter cycle was equal to that of nine switching angles, as shown in Figure 9. Three switching angles are the ideal option for the proposed model. It eliminates the greatest number of harmonics possible, resulting in a THD of only 1.32 percent.When MI is low, higher-order harmonics have more amplitude than lower-order harmonics and vice versa

happens for higher values of MI. Table 3 shows the results of a comparative analysis of several optimization approaches.

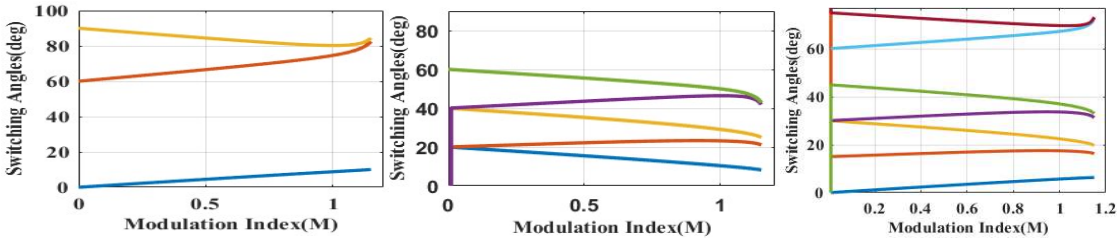

(a) (b) (c)

Figure 9. Behaviour of switching angles vs. modulation index a) for three switching angles b) for five switching angles c) for seven switching angles

Table 3 Comparison of different evolutionary techniques

PSO		**WOA**		**GWO**		**BBO**		**IJFA**	
Weight (w)	0.4	Population matrix	10*5	Population matrix	10*5	Population size	50	Population size	100
Balance factors c_1 , c_2 , c_3 , c_4	1.3,0.6, 1.9, 1.7					Genes in each population	5		
Random variable: r_1 , r_2	0.6, 0.5	Random variable r_1 , r_2	0.7, 0.6	Random variable r_1 , r_2	0.7, 0.6	Elitism value	2	Random variable r_1 , r_2 , r_3 , r_4	0.8,0.6, 0.3,0.7
No. of equations	Low	No. of equations	Low	No. of equations	Low	No. of equations	High	No. of equations	Medium
Complexity	Easy	Complexity	Easy	Complexity	Easy	Complexity	Moderate	Complexity	Moderate
Elapse time (s)	0.43	Elapse time (s)	0.22	Elapse time (s)	0.26	Elapse time (s)	0.34	Elapse time (s)	0.19
THD (%)	2.5	THD (%)	2.98	THD (%)	3.5	THD (%)	3.8	THD (%)	1.32

Figures 10(a), (b) show the behaviour of three switching angles to the modulation index every quarter cycle for an evolutionary algorithm. The switching angles are inversely proportional to the modulation index, and there has been a moderate movement to the origin, as shown in the graph. These angles satisfy the criteria in (23) while also controlling the fundamental component and suppressing harmonics in the output voltage. Both inverters function well in the 0.8-0.87 modulation index region, which explains the choice of three switching angles over others. The comparative plot in Figure 10 (c) depicts the change in THD for different switching strategies at different modulation indices. The amplitudes of voltage harmonics were compared to the standards indicated in Table 4.

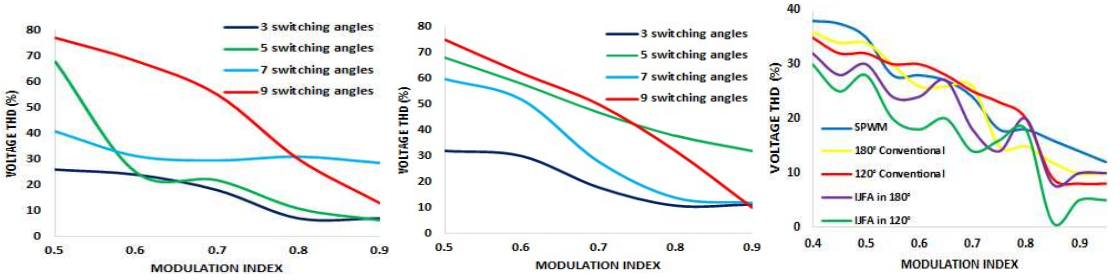

(a) (b) (c)

Figure 10. Voltage output analysis for the variation of THD vs. MI a) IJFA implemented in 180° b) IJFA implemented in 120° c) characteristics of different metaheuristic techniques

Table 4 Comparison of voltage harmonic amplitudes of standards with the proposed techniques

	Standard Reports used										
Voltage harmonics amplitude on grid synchronisation	**b_5**	**b_7**	**b_{11}**	**b_{13}**	**b_{17}**	**b_{19}**	**b_{23}**	**b_{25}**	**b_{29}**	**THD (%)**	

IEC [23]	5	4	3	2.5	1.6	1.2	1.2	1.2	1.06	6.5	
CIGRE WG 36-05 [25]	6	5	3.5	3	2	1.5	1.5	1.5	--	8	
IEEE-1547 and 2030 [22,24]	----------									5	
	Proposed Technique used										
Voltage harmonics amplitude after series compensation (%)	**b_5**	**b_7**	**b_{11}**	**b_{13}**	**b_{17}**	**b_{19}**	**b_{23}**	**b_{25}**	**b_{29}**	**THD (%)**	**Efficiency (%)**
Values for SPWM switching mode	2.4	3.6	2.3	1.9	2.2	4	2	1.8	3.2	6.1	90.8
Values for 180° conventional	2.7	3.27	0.17	3.35	0.5	0.9	4.17	0.08	2.05	5.1	92.3
Values for 120° conventional	1.12	2.5	1.25	1.1	0.22	1.8	1.8	1.12	2.08	4.3	91.2
Values for IJFA in 180°	1.56	1.2	0.45	0.7	0.8	0.43	1.3	0.11	1.9	2.5	92.8
Values for IJFA in 120°	0.49	0.27	0.17	0.15	0.5	0.9	0.57	0.28	0.55	1.32	95.8

7.1 Experimental setup

A per phase system test setup was used to verify the modelling results of the proposed method shown in Figure 11. The solar panels used have a 260-watt capacity, a 35.24-volt open circuit voltage, and an 8.57-amp short circuit current rating. PV panels were used to power both the main and auxiliary inverters at the same time under two separate situations. In the test room, incandescent bulbs were used to create an artificial isolation for consistent irradiance. The PSC was created by adjusting the intense light intensity of 1000 W and covering 20% of it with cardboard, as illustrated in Figure 11. For temperature and irradiation sensing, the LM35 and Pyranometer were used respectively. These signals were amplified using a PIC18F452 controller in a computer interface environment. To trigger the MOSFET of the boost converter, the pulse is amplified using a voltage optocoupler from the (TLP-250H of 1636 series) driver. To drive both inverters, SHEPWM pulses were created using the IJFA algorithm and stored in the PIC18F452 microcontroller. The results were seen in a Digital Storage Oscilloscope using a transformer with a rating of 230/48V, 2A and a nonlinear load of 1A, 0.8 power factor (DSO).

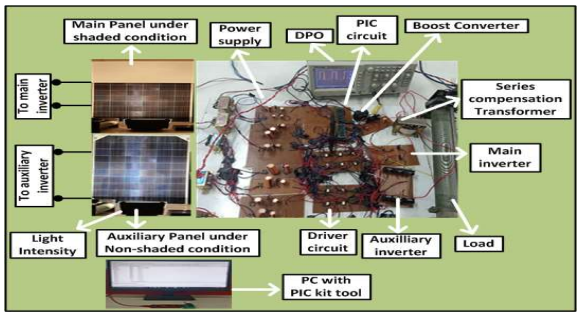

Figure 11. Experimental setup

Figures 12(a), (b) show the gate pulses delivered to switches in the main and compensating inverters using IJFA-based 120° conduction. As the results for the IJFA-based 120° are found to be the best, therefore, its firing pulses have been implemented for the hardware setup. Three switching pulses per quarter cycle have been used for the inverter separately. The output waveforms of the main and auxiliary voltages are shown in Figs. 13(a), (b). In Figure 13 (a), voltage variation can be seen for both uniform and non-uniform isolation. Figure 13 (c) shows the output after series compensation, similar to before PSC. Due to the change in irradiance, voltage variation causes a change in the dc bus which was overcome by an auxiliary inverter. FFT analysis has been shown to manifest a higher number of harmonics present than the latter at an MI of 0.5. Figure 14 (c) shows the FFT analysis at an MI of 0.8. The after-compensation results were improved for MI at 0.8. The amplitude of the targeted harmonics has been lowered by a significant amount. Due to the fact that the experimental setup is in phase, triple-n harmonics are also present. The harmonic order was focused up to the 29th order, as anything beyond that was insignificant. The IJFA, implemented in 120°, eliminates the maximum order of harmonics. For the three-phase system, the THD attained by simulation results was only 1.32%, as shown in Figure 8 (b) and Table 4. The THD for the per phase laboratory experimental prototype was found to be 2.58%,

as shown in Figure 14(c).As a result, it was determined that the simulated and experimental results were completely in accord. Table 5 shows the results of a comparison of existing and proposed designs. It was inferred that the present proposed scheme works better due to the inclusion of novel series compensation, appropriate for industrial and domestic applications.

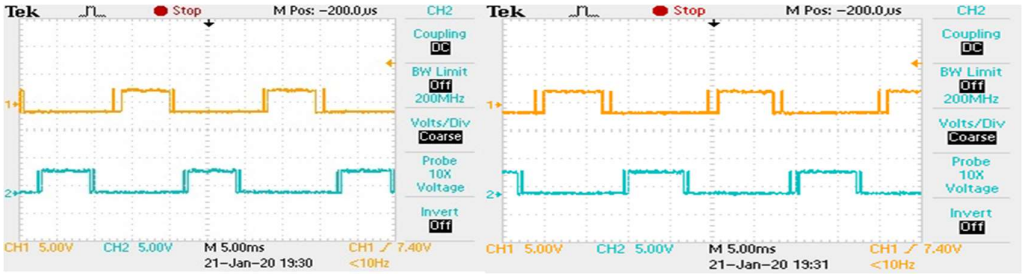

(a) (b)

Figure 12. Gate pulses of switches a) SHEPWM-based 120º conduction in the main inverter (scale: CH1: Y-axis: 5V/div.) b) SHEPWM-based 120º conduction in the auxiliary inverter (scale: CH1: Y-axis: 5V/div.)

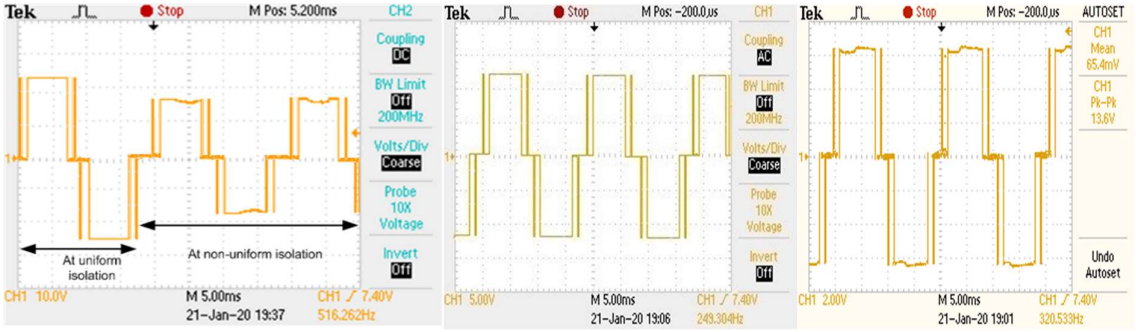

(a) (b) (c)

Figure 13. Output voltage waveform a) SHEPWM based120º conduction in main inverter (scale: CH1: Y-axis: 60V/div.) b) SHEPWM based120º conduction in auxiliary inverter (scale: CH1: Y-axis: 12V/div.) c) at the grid side after series compensation (scale: CH1: Y-axis: 120V/div.)

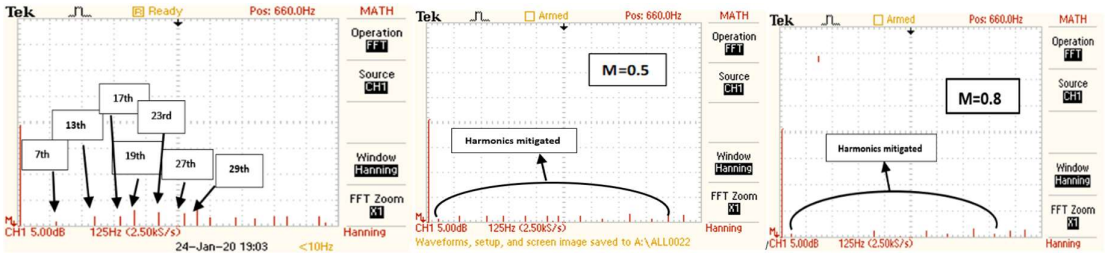

(a) (b) (c)

Figure 14. Voltage harmonics spectra up to the 29th harmonic order a) before series compensation (scale: CH1: Y-axis: 60V/div; X-axis: 250Hz/div) b) after series compensation (scale: CH1: Y-axis: 120V/div; X-axis: 250Hz/div) at MI=0.5.c) at MI=0.8, after series compensation (scale: CH1: Y-axis: 120V/div; X-axis: 250Hz/div).

Table 5
Comparative analysis of existing and proposed schemes

Parameters	**Ref [12]**	**Ref [14]**	**Ref [15]**	**Ref [16]**	**Ref [17]**	**Ref [18]**	**Ref [19]**	**Proposed**
Technique used	UPQC	RBFNN-PI	FPGA	MNR with pattern recognition	Homotopy algorithm	ABC	Filter compensation module	IJFA
Voltage THD (%)	3.71	2.72	16.54	7.25	33.94	3.1	5.1	1.32

8. Conclusion

With the use of series compensation under PSC, it was possible to eliminate harmonics while also improving the voltage profile for the PV integrated grid system. During wider voltage variations, the compensating inverter fulfils the voltage demand on the grid side. The overall THD of the output voltage was reduced to 1.32 percent, which is well within the specifications of IEEE 1547, IEC, and CIGRE WG 36-05. In comparison to existing approaches with changing loads, the proposed IJFA based SHE gives improved results. The experimental results of the prototype have also been presented in support of the simulated outputs. The three switching angles performance was equivalent to nine switching angles per quarter cycle in reducing harmonics, resulting in lower losses and improved system efficiency. A piecewise mixed-model approach has been used to store angles offline in the micro-controller for the online applications. It can be concluded that the current proposed system produces superior results when compared to other existing algorithms and meets all of the paper's objectives.

Acknowledgement

The authors are grateful to Jadavpur University for funding their research via the grant scheme Rashtriya Uchchattar Shiksha Abhiyan (JU - RUSA 2.0). The authors are also grateful to Jadavpur University's Illumination Laboratory for their cooperation.

Ethical Approval

The manuscript is an original research work. This has neither been published previously, nor under consideration for publication elsewhere.

Conflicts of interest

None.

Informed Consent

Approved.

Authorship contribution

The co-authors have helped in supervision and proofreading.

References

[1] Choudhary, Piyush, and Rakesh Kumar Srivastava. "Sustainability perspectives-a review for solar photovoltaic trends and growth opportunities." *Journal of Cleaner Production* 227 (2019): 589-612.

[2] Alsumiri, Mohammed. "Residual incremental conductance based nonparametric MPPT control for solar photovoltaic energy conversion system." *IEEE Access* 7 (2019): 87901-87906.

[3] Rezk, Hegazy, and Ali M. Eltamaly. "A comprehensive comparison of different MPPT techniques for photovoltaic systems." *Solar energy* 112 (2015): 1-11.

[4] Eltamaly, Ali M., M. S. Al-Saud, and A. G. Abo-Khalil. "Performance improvement of PV systems' maximum power point tracker based on a scanning PSO particle strategy." *Sustainability* 12.3 (2020): 1185.

[5] Zhang, Yiying, Maode Ma, and Zhigang Jin. "Comprehensive learning Jaya algorithm for parameter extraction of photovoltaic models." *Energy* 211 (2020): 118644.

[6] Ye, Xiaojia, et al. "Modified Whale Optimization Algorithm for Solar Cell and PV Module Parameter Identification." *Complexity* 2021 (2021).

[7] Eltamaly, Ali M., and Hassan MH Farh. "Dynamic global maximum power point tracking of the PV systems under variant partial shading using hybrid GWO-FLC." *Solar Energy* 177 (2019): 306-316.

[8] Chou, Jui-Sheng, and Dinh-Nhat Truong. "A novel metaheuristic optimizer inspired by behavior of jellyfish in ocean." *Applied Mathematics and Computation* 389 (2021): 125535.

[9] Chou, Jui-Sheng, and Dinh-Nhat Truong. "Multiobjective optimization inspired by behavior of jellyfish for solving structural design problems." *Chaos, Solitons & Fractals* 135 (2020): 109738.

[10] Abdel-Basset, Mohamed, et al. "An improved artificial jellyfish search optimizer for parameter identification of photovoltaic models." *Energies* 14.7 (2021): 1867.

[11] Chou, Jui-Sheng, and Dinh-Nhat Truong. "A novel metaheuristic optimizer inspired by behavior of jellyfish in ocean." *Applied Mathematics and Computation* 389 (2021): 125535.

[12] Sarker, Krishna, Debashis Chatterjee, and S. K. Goswami. "A modified PV-wind-PEMFCS-based hybrid UPQC system with combined DVR/STATCOM operation by harmonic compensation." *International Journal of Modelling and Simulation* 41.4 (2021): 243-255.

[13] Sarker, Krishna, Debashis Chatterjee, and Swapan K. Goswami. "Modified harmonic minimisation technique for doubly fed induction generators with solar-wind hybrid system using biogeography-based optimisation." *IET Power Electronics* 11.10 (2018): 1640-1651.

[14] Sujatha, B. G., and G. S. Anitha. "Enhancement of PQ in grid connected PV system using hybrid technique." *Ain Shams Engineering Journal* 9.4 (2018): 869-881.

[15] Miceli, Rosario, Giuseppe Schettino, and Fabio Viola. "A novel computational approach for harmonic mitigation in PV systems with single-phase five-level CHBMI." *Energies* 11.8 (2018): 2100.

[16] Al-Hitmi, Mohammed, et al. "Selective harmonic elimination in a wide Modulation range using modified Newton–Raphson and pattern generation methods for a multilevel inverter." *Energies* 11.2 (2018): 458.

[17] Ning, Li, et al. "Comparative research of harmonic suppression algorithm of the three-level NPC converter." *The Journal of Engineering* 2019.16 (2019): 1271-1274.

[18] Ramesh, A., and H. Habeebullah Sait. "An approach towards selective harmonic elimination switching pattern of cascade switched capacitor twenty-nine-level inverter using artificial bee colony algorithm." *Microprocessors and Microsystems* 79 (2020): 103292.

[19] Khosravi, N., et al. "Improvement the harmonic conditions of the AC/DC microgrids with the presence of filter compensation modules." *Renewable and Sustainable Energy Reviews* 143 (2021): 110898.

[20] Etesami, Mohammad Hossein, et al. "Enhanced metaheuristic methods for selective harmonic elimination technique." *IEEE Transactions on Industrial Informatics* 14.12 (2018): 5210-5220.

[21] Memon, Mudasir Ahmed, et al. "Selective harmonic elimination in inverters using bio-inspired intelligent algorithms for renewable energy conversion applications: A review." *Renewable and Sustainable Energy Reviews* 82 (2018): 2235-2253.

[22] Cleveland, F. M. "IEC 61850-7-420 communications standard for distributed energy resources (DER)." *2008 IEEE Power and Energy Society General Meeting-Conversion and Delivery of Electrical Energy in the 21st Century*. IEEE, 2008.

[23] Blooming, Thomas M., and Daniel J. Carnovale. "Application of IEEE Std 519-1992 harmonic limits." *Conference Record of 2006 Annual Pulp and Paper Industry Technical Conference*. IEEE, 2006.

[24] Basso, Thomas. *IEEE 1547 and 2030 standards for distributed energy resources interconnection and interoperability with the electricity grid*. No. NREL/TP-5D00-63157. National Renewable Energy Lab. (NREL), Golden, CO (United States), 2014.

[25] Beaulieu, Germain, et al. "Power quality indices and objectives. Ongoing activities in CIGRE WG 36-07." *IEEE Power Engineering Society Summer Meeting,* Vol. 2. IEEE, 2002.

[26] Chatterjee, Debashis. "A novel magnetizing-curve identification and computer storage technique for induction machines suitable for online application." *IEEE Transactions on Industrial Electronics* 58.12 (2011): 5336-5343.